Rigidity Matching between Cells and the Extracellular Matrix Leads to the Stabilization of Cardiac Conduction

AUTHOR(S):

Hörning, Marcel; Kidoaki, Satoru; Kawano, Takahito; Yoshikawa, Kenichi

CITATION:

Hörning, Marcel ...[et al]. Rigidity Matching between Cells and the Extracellular Matrix Leads to the Stabilization of Cardiac Conduction. Biophysical Journal 2012, 102(3): 379-387

ISSUE DATE:

2012-02

URL:

http://hdl.handle.net/2433/154765

Rigidity-matching between cells and the extracellular matrix leads to the stabilization of cardiac conduction

Marcel Hörning
Department of Physics
Graduate School of Science
Kyoto University, Japan

Satoru Kidoaki
Division of Biomolecular Chemistry
Institute for Materials Chemistry and Engineering
Kyushu University, Fukuoka, Japan

Takahito Kawano
Division of Biomolecular Chemistry
Institute for Materials Chemistry and Engineering
Kyushu University, Fukuoka, Japan

Kenichi Yoshikawa[1]
Department of Physics
Graduate School of Science
Kyoto University, Japan

December 31, 2011

[1]Department of Physics, Graduate School of Science, Kyoto University, Kyoto, Kyoto 606-8502, Japan, Tel.:(0081)75-753-3812, Fax:(0081)75-753-3779

Abstract

Bio-mechanical dynamic interactions between cells and the extracellular environment dynamically regulate physiological tissue behavior in living organisms, such as that seen in tissue maintenance and remodeling. In this study, the substrate-induced modulation of synchronized beating in cultured cardiomyocyte tissue was systematically characterized on elasticity-tunable substrates to elucidate the effect of bio-mechanical coupling. We found that myocardial conduction is significantly promoted when the rigidity of the cell culture environment matches that of the cardiac cells (4 kilopascals). The stability of spontaneous target wave activity and calcium transient alternans in high frequency-paced tissue were both enhanced when the cell substrate and cell tissue showed the same rigidity. By adapting a simple theoretical model we reproduced the experimental trend on the rigidity matching for the synchronized excitation. We conclude that rigidity-matching in cell-to-substrate interactions critically improves cardiomyocyte-tissue synchronization, suggesting that mechanical coupling plays an essential role in the dynamic activity of the beating heart.

Key words: cell rigidity, tissue engineering, calcium instability, alternants, cell coupling, pacemaker, excitability, synchronization, fibrillation, arrhythmias

Introduction

Cardiovascular diseases are a major cause of death in modern society and affect millions of people worldwide. Studies on common potentially fatal cardiac diseases have high priority in the scientific and medical communities. Reentries are known to be responsible for many dangerous cardiac arrhythmias and are precursors of ventricular fibrillation that leads to sudden death (1–4). Thus, it is important that we understand how such undesired wave dynamics originate. To reveal underlying mechanisms and causes, different models of heart function are generally used, such as in vivo and in vitro systems of cardiac tissue. While in vitro cultures often show generic rather than realistic features, they are easy to maintain and observe. Cardiac tissue culture is a type of in vitro experimental system that uses the hearts of neonatal mammals to reengineer heart tissue on a two-dimensional substrate. Generally, it is used to examine the activities of newly developed medical drugs (5), the nonlinear activity of wave dynamics (4, 6), and stem-cell development (7).

Adhesion is an important cell property that is not only controlled by biochemical mechanisms, but is also regulated by the ability of cells to sense their mechanical and molecular microenvironment to determine the structural organization within the cell (8–10), such as the extracellular matrix, cytoskeleton and force generation through molecular motors (11, 12). Typical examples include cell migration (13, 14) and the differentiation of stem cells (4, 15). Thus, substrate rigidity plays an important role in in vitro experiments to realistically model the extracellular matrix as in in vivo experiments exhibit.

Substrate rigidity can be modulated by the use of different types of soft gels such as agar gels (16) and fibrin gels (17). A gel that was recently introduced for tissue engineering is elasticity-tunable photo-curable styrenated gel (18, 19), the local rigidity of which can be precisely adjusted by controlling the duration of irradiation with visible light. The resulting gels exhibit rigidities from a few kPa up to 1 MPa, and hence open the possibility to mimic the extracellular matrix in the cell environment.

In this study we systematically investigated the influence of rigid substrates to the calcium conduction of confluent cardiomyocyte monolayers of neonatal rats. The records of spontaneous calcium-waves were analyzed by obtaining the power-spectrum for substrates with different rigidity. The main entrainment-frequency showed an increase with the increase in substrate rigidity, and the entrainment stability of spontaneous originated waves become maximized when the substrate rigidity and cell rigidity (ca. 4 kilopas-

cals) matches.
For verification of the effect of rigidity matching, the threshold of calcium alternans was analyzed in rapid rate-paced tissues. It was found that when the rigidity of the cell culture substrate matches that of the cardiac cell tissue, the threshold of the period to induce calcium alternants increases significantly.
Our experimental obtained results suggest that when tissue and substrate have the same rigidity the cell-to-substrate interactions critically improves synchronization features in cardiomyocyte-tissue.
For clarification of the experimental results, additionally we adapted a simple excitable numerical model to simulate the cell-substrate interaction. Despite the simple nature of the numerical model, our model reproduces the essential features in our experiment by taking mechanical cell-coupling into account.

Methods

Cell isolation

Primary cell cultures of neonatal rat ventricular myocytes were prepared as described previously (20). Briefly, hearts isolated from 2-day-old Wistar rats were minced and treated with collagenase. The isolated cells were collected by centrifugation and preplated for 1 h. After the supernatant was collected again, the cells were plated on 18-mm-diameter glass or gel-prepared coverslips coated with fibronectin (12 μg/ml) at a cell density of 2.6×10^3 cells/mm^2. Cell constructs were incubated in Dulbecco-modified Eagle Medium with 10% fetal bovine serum, and 1% penicillin streptomycin for 24 hours under humidified conditions at 37°C and 5% CO2. The medium was replaced by a contraction medium, which consisted of minimum essential medium with 10% calf serum, 1% penicillin streptomycin, and Cytosine Arabino-Furanoside (ARA-C), a proliferation inhibitor, to minimize the number of fibroblasts (21, 22).
All animal protocols were carried out in strict accordance with the guidelines for animal experimentation from the Animal Research Committee, Kyoto University. The protocol was approved by the Animal Research Committee, Kyoto University.

Immunofluorescence

Observations were performed 4 days after plating. Cells were labeled with the Ca^{2+}-sensitive fluorescent dye Fluo-8 (ABD Bioquest, Fluo-8 AM). The medium was replaced with Tyrode solution at room temperature. The cells were studied within 2 h after loading.

Photo-curable gel fabrication

Photocurable styrenated gelatin was prepared as previously described (23). Styrenated gelatin (30 wt%) and sulfonyl-camphorquinone (Toronto Research Chemicals, Canada; 2.5 wt% of gelatin) were mixed in PBS. The mixture was centrifuged to remove the colloidal coagulations. The photocurable gel solution was spread between the previously prepared vinyl-silanized glass substrate and raw glass substrate coated with poly(N-isopropylacrylamide) for easy detachment, which were kept under 45 C. The sample was than illuminated with visible light at 100mW/cm2 (measured at 568nm) for 150-300s. A metal halide light source (MME-250; Moritex Corp.,Tokyo, Japan) was used. Light intensity was measured using a photodiode power meter (S120C, ThorLabs, Japan). Finally, the hardened gel was detached from the raw glass substrate in PBS and then kept in PBS overnight under incubation and shaking conditions to remove unreacted sol and make it swell sufficiently.

Determination of rigidity

The rigidity of gels and cell tissue was determined by nano-indentation analysis by atomic force microscopy (AFM). Indentation-force measurements were performed by AFM (NVB100; Olympus Optical Co.Ltd., Tokyo, Japan; AFM controller & software, Nanoscope IIIa; Veeco Instruments, CA, USA) using a silicon-nitride cantilever with a pyramidal tip and a nominal spring constant of 0.02 N/m (OMCL-TR400PSAHW, Olympus Optical Co. Ltd. Tokyo, Japan) in PBS. The Young's modulus, E, of the obtained force-indentation curves was analyzed by nonlinear least-squares fitting to the Hertz model (24, 25) considering the case of a conical indenter:

$$F = \frac{2E}{\pi \tan\alpha \,(1-\mu^2)}\delta^2 \tag{1}$$

where the semi-vertical angle is $\alpha = 30^\circ$ and the Poisson ratio is $\mu = 0.5$. A more detailed description on the nano-indentation method is provided in the supplemental material (see Fig. S1 in the Supporting Material).

Time-lapse and image acquisition

Fluorescence was observed with an inverted microscope (IX-70; Olympus, Tokyo Japan) with a X2.0 magnification objective lens (PLAPON, N.A.=0.08, Olympus) in combination with a X0.35 intermediate lens (26). Raw images were obtained with an electron-multiplying CCD camera (iXon DV887ECS-UVB; Andor) with 64x64 pixels at a 14-bit resolution with 200 frames/s after 8x8 binning for the conduction velocity and calcium alternans measurements, and 128x128 pixels with 50 frames/s after 4x4 binning for measurements of spontaneous activation dynamics. High-magnification images were obtained by confocal laser scanning fluorescence microscopy (Carl Zeiss LSM510) using a X20 magnification objective lens (UPlanSApo, N.A.=0.75, Olympus).

Electrical Stimulation

Electrical stimulation of 6V was applied with 10-ms bipolar pulses delivered through 1 mm-spaced platinum electrodes on the edge of the sample without touching the tissue. The pacing period was decreased systematically from 700ms in steps of 50ms and 10ms, respectively, until calcium instabilities could be recognized (see Fig. 1)).

Data analysis

Activation time mapping and data obtained from conduction velocity measurements were processed by ImageJ image-analysis software (W. Rasband [1997-2006] Url: http://rsb.info.nih.gov/ij/) with custom plug-ins as previously introduced (27). Data regarding spontaneous activation dynamics were analyzed by MATLAB (R2010a, The MathWorks) with custom programs.

Results

We cultured neonatal cardiac cell tissue on microelastic gel surfaces that spanned the range of cell rigidity found during the developmental process in cardiac culture [11 gel rigidities between 2.3 kPa $\sim$ 10.2 kPa, and glass as a control] (25). In this approach, the wave activity of a large collection of cell cultures is recorded (n = 33) and a power spectrum is obtained by Fourier transformation. Figure 2 A and B exemplarily show two single-pixel

recorded cytosolic-calcium transients and normed frequency spectra of confluent tissue for constant entrained activity and erratic activity (fast activity followed by periods of quiescence), respectively. Both forms of activity are found in tissue cultures of different substrate rigidities. The unnormalized power spectra of all of the experimental samples, regardless of substrate rigidity, are summed over all single pixel recordings (shown similarly in Fig. 1B) of all experiments to a combined spectrum and subsequently scaled to its maximum value that is approximately at 710 ms (Fig. 2C). Three cycle length (CL) bands of wave activity are distinct and numbered serially: ① low-period activity (CL $>$ 0.9 sec) due to occasional activity delays, ② high-period wave bursts (CL = 0.6 sec $\sim$ 0.9 sec) corresponding to the region with the main cycle length band, and ③ rare events of extremely high-frequency bursts (CL = 0.3 sec $\sim$ 0.6 sec).

Further, we determined the main cycle length of each sample for the lower threshold of wave activity (CL $<$ 710 ms) depending on the cell rigidity. We found a linear dependency between lower rigidities (m = 10 ms/kPa) and increasing dispersion for greater rigidities when we considered the minimum cycle length for each rigidity (Fig. 2D). This suggests that the minimum main cycle length is proportional to the adhesion strength of cells, since the adhesion strength increases monotonically with increasing substrate rigidity, and the strongest adhesion occurs on glass (15).

We obtained the combined power spectrum depending on rigidity to evaluate the underlying relation between substrate rigidity and the frequency (CL) of natural activation sites (Fig. 2E). Each obtained power spectrum was normalized by integrating over its area, and subsequently all rigidity dependent power spectra were scaled to the highest exhibited frequency occurrence. We found that lower rigidities ($\leq$4.2 kPa) show pronounced frequency (CL) domains, however, the wave activity on gels with greater rigidities show a broad distribution of wave frequencies (CL). This result corresponds well with the cell rigidity (4.4 $\pm$ 0.6) kPa that is determined by AFM indentation measurements similarly to the rigid substrates. The cell rigidity marks the threshold between the pronounced frequency domains and the broad frequency distribution of soft and hard rigidities, respectively. Figure 2F shows the maxima of the combined power spectra depending on the substrate rigidity that the tissue is cultured on. The maximum at 4.2 kPa corresponds well with the cell rigidity similar to that with Fig. 2E. The strong difference between tissue cultured on soft and hard substrates is due to the difference in the power spectrum. Higher values indicate more constant beating-frequencies than lower values as it is shown representative in Fig. 2A and B, respectively. Thus, cardiac cells beat most constantly

when cardiac tissue is cultured on substrates that exhibit the the same or lower rigidity as the cell-tissue.

To measure the cycle length distribution we obtained the power spectra by Fourier transformation (FT), rather than defining an arbitrary intensity level and measuring the duration from activation to activation as it has been done previous studies (28). Both methods lead to comparable results but exhibit pros and cons. One advantage of using FT is that it can detect also low intensity peaks that may keep undetected by utilizing a constant intensity level. However, detailed information such as calcium transient duration (CTD) and calcium transient interval (CTI) are not able to measure using FT. For comparison of both methods we prepared the to Fig. 2E corresponding cycle length distribution (see Fig. S3A in the Supporting Material). Both plots show quantitatively the same distribution considering that the frequency f = 1/ CL, respectively.

To emphasize the found effect, we extracted the calcium transient duration (CTD) and calcium transient interval (CTI) of each wave to show the CTD and CTI interaction at an intensity level of 50%. The CTI and CTD for calcium signaling is performed in a comparable way as the action potential duration (APD) and diastolic interval (DI) measurements for the membrane potential of cardiac cells (29, 30) (see Fig. S2A in the supporting material). Figure 3A-C show the relative CTD-CTI occurrence in a normalized histogram for all substrates, soft substrates with rigidities smaller than 4.25 kPa, and hard substrates with rigidities larger than 4.25 kPa, respectively. The difference between Fig. 3B and Fig. 3C shows clearly the stabilization of the conduction system when the substrate rigidity is softer than the cell rigidity. Larger substrate rigidities lead to a broad distribution of CTD-CTI values, however, smaller rigidities lead to a focused CTD-CTI relationship with an average CTD=160ms and CTI=270ms. This effect can be emphasized by the cycle length distribution for soft and hard substrate rigidities, respectively (see Fig. 3D). Tissue that is cultured on soft substrates (red bars) exhibited a lower CL distribution than that of tissues cultured on hard substrates (green bars). The cycle length standard deviation (CL-STD) of each rigidity shows the same trend (see Fig. S3B in the supporting material). Tissue that is cultured on soft substrates exhibit lower CL-STD than of tissues cultured on on hard substrates.

We next focus on the role and effect of wave conduction in tissues cultured on gels rigidities close to 4 kPa [6 gel rigidities from 2.3 kPa to 5.4 kPa, and glass]. We performed independent measurements of conduction speed for an equally large collection of samples (n=31). We obtained the restitution properties of each sample by electric high-frequency stimulation

at the edge of the tissue [T = 700ms - 250ms] (see Fig. 1). Under the experimental conditions in the present study at room temperature, cardiac tissue exhibited strong calcium transient alternans (Fig. 4A), which led to alternating wave propagation at high-frequency entrained waves (31, 32). We extracted the CTD and CTI of each wave at an intensity level of 50% as performed previously (see also Fig. S2A in the supporting material) to investigate wave-to-wave interaction (Fig. 4B). Depending on the activation time of the wave, CTD varied linearly while the pacing period T remained constant for higher pacing periods (T=CTD+CTI) (33). If we define the variation of CTI, Γ, as a generic function of the pacing period, T, we can determine the critical pacing period, T_c, by

$$\Gamma = \alpha \exp\left(-\beta\left(T - T_c\right)\right) + \Gamma_0 \tag{2}$$

where Γ_0 is the average variance of CTI, and α and β are parameters. Thus, we could quantify T_c for each tissue preparation as a function of substrate rigidity (Fig. 4D). The advantage of using this approach is that T_c can be estimated more precise when located between subsequent measurements. We found that T_c is increased at a substrate rigidity of approximately 4 ± 1 kPa. Analyzing the conduction velocities with calcium transient amplitude (CTA) in a similar manner as in previous studies (31, 34, 35) lead to comparable T_c with an increase at a substrate rigidity of 4 kPa, however the standard deviation showed much larger deviations (see Fig. S2 in the supplemental material). This result corresponds well with the independent result obtained for the spontaneous target wave activity, where the highest activity was also found at approximately 4 kPa. Although we found that cytosolic calcium alternans is elevated toward larger periods when the substrate rigidity and cell rigidity matches, we could not observe any significant change in the conduction velocity when the tissue is entrained with the pacing period of 700ms.

Numerical Simulations on the mechanical resonance between cells and substrate

A generic numerical model of FitzHugh-Nagumo (FHN) type was adapted to simulate the essential of the dynamical feature of interaction between cells and substrate (36, 37). The FHN-equations were numerically solved by a Runge-Kutta 4th order explicit integration scheme considering dx=0.1, dt=0.2 and D=0.01 for a one-dimensional array:

$$\dot{u} = D\partial_{xx}u + [u(u-1)(\alpha - u) - v] + I_n + I_c \tag{3}$$

$$\dot{v} = \varepsilon\left(\beta u - \gamma v - \eta\right) \quad , \tag{4}$$

where u and v are the activator and inhibitor, respectively, I_n is Gaussian noise with a standard deviation 0.017 (38) to induce a more natural environment that may cause wave failure, α=0.1, β=0.5, γ=1.0, and ε=0.01. Excitable and oscillatory cells are distinct by the parameter η either 0.0 or 0.1, respectively, where the first 10 units are set to be oscillatory mimicking a natural pacemaker. Further, we introduce a non-diffusive coupling term I_c, to mimic the basic function of stress-activated ion-channels, that is considered as a monotonic decaying arbitrarily defined function of the distance between neighboring cells. Thus, we define I_c as

$$I_c(u_x) = \Theta\left(u_x > u_{th}\right) \times \sum_{i}^{i \neq x} \left[u_i + f(E_s, E_c)\right] \tag{5}$$

with

$$f(E_s, E_c) = c_1 \exp\left(-\frac{|i-x|-1}{c_2 + \left|E_c^2\left(E_c^2 + |E_s^2 - E_c^2|\right)^{-1} - c_3\right|}\right) \quad , \tag{6}$$

where Θ is a Heaviside step-function, which triggers coupling of neighboring cells only if the cell is in the excited state, thus contract. E_s is the substrate rigidity and E_c is the cell rigidity. Parameters are set arbitrary to c_1=0.002, c_2=0.1, and c_3=0.3. No-flux boundary conditions are assumed.
Equation 6 is defined having two characteristics. When the elastic moduli (rigidities) E_s and E_c are equal, the coupling is strongest, thus, independent of elastic moduli since Eq. 6 reduces to

$$f = c_1 \exp\left(-\frac{|i-x|-1}{c_2 + c_3}\right) \quad , \tag{7}$$

so that the parameters $c_{1,2,3}$ define the strength of coupling. On the other hand the denominator shows a strong asymmetry for smaller and larger E_s, respectively, due to the choice of the quadratic elasticities.
Figure 5(A-C) shows exemplarily in respect to the undisturbed system (A) the influence of noise (B) and long-range coupling (C) for a 100 unit lattices, respectively. The influence of noise leads to failure of wave propagation in the excitable part of lattices. Whereas, the coupling decreases failure probability of waves, resulting in a more stable wave train. In Figure 5D we show the power spectrum depending on rigidity to evaluate the underlying relation between substrate rigidity and the frequency of wave train, which reproduces the experimental trend (Fig. 2F). The power spectra were analyzed in the same manner as it was explained for the experimental data.

First the power spectra were obtained from a single recorded space unit in the excitable region and then normalized to the maximum of all power spectra. In the simulation, the cell rigidity was set to 4 kPa.

Discussion

Enhancement of the stability of the target wave activity and an increase in the critical period of calcium transient alternans were observed at the same substrate rigidity, which corresponded to a cell rigidity of 4.4 ± 0.6 kPa, as that obtained by measuring the cell rigidity by the atomic force microscope indentation method (25, 39, 40) in control tissue on glass cover slips on the fourth day of culture (observation day) [3 samples at 3 different locations]. The cell rigidity obtained by this method is in good agreement with the obtained result, and confirms independently that cardiac cells exhibit an optimized and more stable state of spontaneous wave activity when the substrate rigidity matches or is lower than the cell rigidity. Thus, the cell rigidity can be interpreted as a critical point of stability, since an increase of the substrate rigidity yield to an decrease in stability so that spontaneous activity becomes erratic, as Fig. 2E and Fig. 3 suggest.

Our results indicate that the rigidity of the extracellular environment of cells plays a significant role in determining cardiac conduction dynamics. The interaction of biomechanical and cell physiological activity exhibits a resonance effect when the rigidity of the extracellular matrix is equal to the rigidity of cardiac cell tissue. We observed an increase in the stability of target waves that led to stabilization of the main entrained activation frequency in the system when the substrate rigidity matches or is lower than the cell rigidity, which also indicates an effect on the intracellular activity (41). Further, we found that the critical period of calcium transient alternans increases when cell rigidity is equal or less the substrate rigidity, since it is induced at a longer pacing period, that is associated with a more diseased state, such as heart failure (42). However, although calcium transient alternans is induced at a longer pacing period, it does not lead to a diseased state, but a change in tissue properties considering cardiac tissue. Thus, together with the finding of the stabilization of spontaneous wave activity, we can speak of a stabilization of cardiac conduction.

The observed resonance effect between tissue and substrate can be explained by the changes induced in cell morphology during tissue maturation due to the difference in adhesion area (9), and thus also in the cohesion area between cells. Although speculative, we believe that this may regulate the

intracellular morphology of cells by adjusting the actin skeleton and gap-junction density between cells. Thus, the interaction between force actuation and conduction may regulate to the extent to which cell functionality is optimized when cell rigidity is equal or less the substrate rigidity. The mechanical interaction between cell and substrate is considered to play a dominant role on the excitable system, resulting in stabilized spontaneous wave activity for lower rigidities (see Figs. 2F and 3D) and induced calcium alternans at larger pacing periods (see Fig. 4D). A simple theoretical model is discussed that reproduces the essential feature of the experimental results (Fig. 5). We believe that by additionally introducing cell orientation, the resonant effect may increase so that the conduction system will improve toward the quality seen in in vivo systems.

Here, we provide insights into the stability of spontaneous target wave activity and calcium transient alternans in high frequency-paced tissue, which are determined by biomechanical interactions between cells and the extracellular environment that dynamically modulate the physiological tissue behavior in living cells. Our results suggest that the quality of in vitro studies on cardiac tissue culture can be dramatically improved so that they are more similar to those performed in vivo by adjusting the substrate rigidity, so that the extracellular matrix successfully mimics the extracellular environment of cardiac tissue (5, 7, 43, 44).

Our results should contribute to in vitro studies on the cardiac system. Although the underlying cell-physiological mechanism and the intracellular cell morphology in confluent cardiac tissue remain to be elucidated, our results support the hypotheses that decreased rigidity preserves not only stem cells (7) but also enhances cell development by altering the cell morphology (9), resulting in cytoskeletal rearrangement and altered signaling. Our results suggest that mimicking the extracellular environment in in vitro cultures can cause the tissue culture to more closely approximate native cell functionality and may help improve reengineering heart tissues for regeneration of diseased hearts that uses extracellular matrix proteins such as Matrigels (45).

Acknowledgement

We thank Dr. Thasaneeya Kuboki, Dr. Masatoshi Ichikawa, Dr. Amgad Squires, Dr. Valentin Krinsky and Yukinori Nishigami for their valuable support and discussions. This work was supported by the Japan Science and Technology Agency, CREST (Team Kageyama), a JSPS Research Fellowship for young scientists (21-102), and in part by the Management Ex-

penses Grants for National Universities Corporations from the Ministry of Education, Culture, Sports, Science and Technology of Japan (MEXT).

References

1. Winfree, A. T., 1972. Spiral Waves of Chemical Activity. *Science* 175:634–636.

2. Winfree, A. T., 2004. Electrical turbulence in three-dimensional heart muscle. *Science* 266:1003–1006.

3. Weiss, J., Z. Qu, P. Chen, S. Lin, H. Karagueuzian, H. Hayashi, A. Garfinkel, and A. Karma, 2005. The Dynamics of Cardiac Fibrillation. *Circulation* 112:1232–1240.

4. Jalife, J., 2000. Ventricular Fibrillation: Mechanisms of Initiation and Maintenance. *Annual Review of Physiology* 62:25–50.

5. Elliott, N., and F. Yuan, 2011. A review of three-dimensional in vitro tissue models for drug discovery and transport studies. *Journal of Pharmaceutical Sciences* 100:59–74.

6. Haïssaguerre, M., P. Jaïs, D. Shah, A. Takahashi, M. Hocini, G. Quiniou, S. Garrigue, A. L. Mouroux, P. L. Métayer, and J. Clémenty, 1998. Spontaneous initiation of atrial fibrillation by ectopic beats originating in the pulmonary veins. *The New England Journal of Medicine* 339:659–666.

7. Gilbert, P., K. Havenstrite, K. Magnusson, A.Sacco, N. Leonardi, P. Kraft, N. Nguyen, S. Thrun, M. Lutolf, and H. Blau, 2010. Substrate Elasticity Regulates Skeletal Muscle Stem Cell Self-Renewal in Culture. *Science* 329:1078–1081.

8. Besser, A., and U. Schwarz, 2007. Coupling biochemistry and mechanics in cell adhesion: a model for inhomogeneous stress fiber contraction. *New Journal of Physics* 9:425.

9. Yoshikawa, H. Y., F. F. Rossetti, S. Kaufmann, T. Kaindl, J. Madsen, U. Engel, A. L. Lewis, S. P. Armes, and M. Tanaka, 2011. Quantitative Evaluation of Mechanosensing of Cells on Dynamically Tunable Hydrogels. *Journal of the American Chemical Society* 133:1367–1374.

10. Schwarz, U., 2007. Soft matters in cell adhesion: rigidity sensing on soft elastic substrates. *Soft Matter* 3:263–266.

11. Discher, D., P. Janmey, and Y. Wang, 2005. Tissue cells feel and respond to the stiffness of their substrate. *Science* 310:1139–1143.

12. Vogel, V., and M. Sheetz, 2006. Local force and geometry sensing regulate cell functions. *Nature Reviews Molecular Cell Biology* 7:265–275.

13. Carter, S., 1965. Principles of Cell Motility: The Direction of Cell Movement and Cancer Invasion. *Nature* 208:1183–1187.

14. Lo, C., H. Wang, M. Dembo, and Y. Wang, 2000. Cell movement is guided by the rigidity of the substrate. *Biophysical Journal* 79:144–152.

15. Engler, A. J., M. A. Griffin, S. Sen, C. G. Bönnemann, H. L. Sweeney, and D. E. Discher, 2004. Myotubes differentiate optimally on substrates with tissue-like stiffness: pathological implications for soft or stiff microenvironments. *The Journal of Cell Biology* 166:877–887.

16. Grando, S. A., A. M. Crosby, B. D. Zelickson, and M. V. Dahl, 1993. Agarose Gel Keratinocyte Outgrowth System as a Model of Skin Reepithelization: Requirement of Endogenous Acetylcholine for Outgrowth Initiation. *Journal of Investigative Dermatology* 101:804–810.

17. Ye, Q., G. Zünd, S. Jockenhoevel, S. P. Hoerstrup, A. Schoeberlein, J. Grunenfelder, and M. Turina, 2000. Tissue engineering in cardiovascular surgery: new approach to develop completely human autologous tissue. *European Journal of Cardio-Thoracic Surgery* 17:449–454.

18. Kidoaki, S., and T. Matsuda, 2008. Microelastic gradient gelatinous gels to induce cellular mechanotaxis. *Journal of Biotechnology* 133:225–230.

19. Kawano, T., and S. Kidoaki, 2011. Elasticity boundary conditions required for cell mechanotaxis on microelastically-patterned gels. *Biomaterials* 32:2725–2733.

20. Matoba, S., T. Tetsuya, N. Keira, A. Kawahara, and K. Akashi, 1999. Cardioprotective Effect of Angiotensin-Converting Enzyme Inhinition Against Hypoxia/Reoxygenation Injury in Cultured Rat Cardiac Myocytes. *Circulation* 99:817–822.

21. Haddad, J., M. Decker, L. Hsieh, M. Lesch, A. Samarel, and R. Decker, 1988. Attachment and maintenance of adult rabbit cardiac myocytes in primary cell culture. *American Physiological Society* 255:19–27.

22. Boateng, S., T. Hartman, N. Ahluwalia, H. Vidula, T. Desai, and B. Russell, 2003. Inhibition of fibroblast proliferation in cardiac myocyte cultures by surface microtopography. *American Journal of Cell Physiology* 285:171–182.

23. Okino, H., Y. Nakayama, M. Tanaka, and T. Matsuda, 2001. In situ hydrogelation of photocurable gelatin and drug release. *Journal of Biomedical Materials* 59:233–245.

24. Hertz, H., 1881. Ueber die Beruehrung fester elastischer Koerper. *Journal fuer die reine angewandte Mathematik* 92:156–171.

25. Sneddon, I., 1965. The Relation between Load and Penetration in the Axisymmetric Boussinesq Problem for a Punch of Arbitrary Profile. *International Journal of Engineering Science* 3:47–57.

26. Entcheva, E., and H. Bien, 2005. Macroscopic optical mapping of excitation in cardiac cell networks with ultra-high spatiotemporal resolution. *Biophysics and Molecular Biology* 92:232–257.

27. Isomura, A., M. Hörning, K. Agladze, and K. Yoshikawa, 2008. Eliminating Spiral Waves Pinned to an Anatomical Obstacle in Cardiac Myocytes by High-Frequency Stimuli. *Physical Review E* 78.

28. Rohr, S., 1990. A computerized device for long-term measurements of the contraction frequency of cultured rat heart cells under stable incubating conditions. *European Journal of Physiology* 416:201–206.

29. Elharrar, V., and B. Surawicz, 1983. Cycle length effect on restitution of action potential duration in dog cardiac fibers. *American Journal of Physiology* 244:782–792.

30. MacFarlane, N., A. Rankin, and M. McIntosh, 1997. Brief exposure to hydrogen peroxide shortens action potential and calcium transient durations in left ventricular endocardial myocytes isolated from a rabbit coronary artery ligation model of heart failure. *JOURNAL OF PHYSIOLOGY-LONDON* 501P:138–138.

31. Clusin, W., 2008. Mechanisms of calcium transient and action potential alternans in cardiac cells and tissues. *American Journal of Physiology Circ. Physiol.* 294:1–10.

32. J. Lechleiter, E. P., S. Girard, and D. Clapham, 1991. Spiral calcium wave propagation and annihilation in Xenopus laevis oocytes. *Science* 252:123–126.

33. Fenton, F., E. Cherry, H. Hastings, and S. Evans, 2002. Multiple mechanisms of spiral wave breakup in a model of cardiac electrical activity. *Chaos* 12:852–892.

34. Lee, H.-C., R. Mohabir, N. Smith, M. Franz, and W. Clusin, 1988. Effect of Ischemia on Calcium-Dependent Fluorescence Transients in Rabbit Hearts Containing Indo 1. *Circulation* 78:1047–1059.

35. Jia, H. Bien, and E. Entcheva, editors, 2007. Spatially discordant alternans (SDAs) in intracellular calcium in paced quasi-1D cardiac tissue. IEEE; EMB; AIChE, 2007 IEEE 33RD ANNUAL NORTHEAST BIOENGINEERING CONFERENCE.

36. FitzHugh, R., 1961. Impulses and physiological states in theoretical models of nerve membrane. *Biophysical Journal* 1:445–466.

37. Gray, R., 2002. Termination of spiral wave breakup in a Fitzhugh–Nagumo model via short and long duration stimuli. *Chaos* 12:941–951.

38. Lindner, B., J. Garcia-Ojalvo, A. Neiman, and L. Schimansky-Geier, 2004. Effects of noise in excitable systems. *Physics Reports* 392:321–424.

39. Hanson, B., P. Sutton, N. Elameri, M. Gray, H. Critchley, J. S. Gill, and P. Taggart, 2009. Interaction of Activation–Repolarization Coupling and Restitution Properties in Humans. *Circulation: Arrhythmia and Electrophysiology* 2:162–170.

40. Weisenhorn, A. L., M. Khorsandi, S. Kasas, V. Gotzos, and H.-J. Butt, 1993. Deformation and height anomaly of soft surfaces studied with an AFM. *Nanotechnology* 4:106–113.

41. Xie, L., G. Clunn, J. Lymn, and A. Hughes, 1998. Role of intracellular calcium ([Ca2+]i) and tyrosine phosphorylation in adhesion of cultured vascular smooth muscle cells to fibrinogen. *Cardiovascular Research* 39:475–484.

42. Wilson, L. D., D. Jeyaraj, X. Wan, G. S. Hoeker, T. H. Said, M. Gittinger, K. R. Laurita, and D. S. Rosenbaum, 2009. Heart failure

enhances susceptibility to arrhythmogenic cardiac alternans. *Heart Rhythm* 6:251–259.

43. Engler, A. J., C. Carag-Krieger, C. P. Johnson, M. Raab, H.-Y. Tang, D. W. Speicher, J. W. Sanger, J. M. Sanger, and D. E. Discher, 2008. Embryonic cardiomyocytes beat best on a matrix with heart-like elasticity: scar-like rigidity inhibits beating. *Journal of Cell Science* 121:3794–3802.

44. Collinsworth, A., S. Zhang, W. Kraus, and G. Truskey, 2002. Apparent elastic modulus and hysteresis of skeletal muscle cells throughout differentiation. *American Journal of Cell Physiology* 283:C1219–C1227.

45. Zimmermanna, W.-H., I. Melnychenkoa, and T. Eschenhagen, 2004. Engineered heart tissue for regeneration of diseased hearts. *Biomaterials* 25:1639–1647.

Figure Legends

Figure 1.

Activation-time maps (left) and single pixel recording of the cytosolic calcium of confluent cardiac tissue culture on glass (A) and on gel-substrate with a rigidity of 4.2 kPa (B). Single pixel recordings are shown for 700ms and 280ms-entrained high-frequency paced tissues that exhibit stable calcium transient alternans for 280ms-entrained tissues.

Figure 2.

Spontaneous wave activity shows most constant activity when cardiac cell tissue is cultured on soft substrates of equal rigidity. (A and B) Examples of two single-pixel recorded cytosolic-calcium transients and normed frequency spectra of confluent tissue cultured on 3.5 kPa gel substrates showing a constant transient and transient with delays, respectively. We confirmed that tissue cultured on different gel substrates or glass shows similar patterns. (C) Relative cycle length distribution of all samples (n=33, two 60-sec records) shows distinct cycle length (CL) bands: ① high-period activity (CL $>$ 0.9 sec) due to occasional activity delays, ② low-period wave bursts (CL = 0.6 sec $\sim$ 0.9 sec) corresponding to the region with the main frequency band, and ③ rare events of extremely high-frequency bursts (CL = 0.3 sec $\sim$ 0.6 sec). Most CLs are observed at a period of 710 ms. (D) A linear increase in the minimum spontaneous CL with maximum occurrence of target waves is shown. The figure-inlet shows CL of spontaneous waves with maximum amplitude of each sample. (E) Map of combined power spectrum depending on substrate rigidity and wave frequency (CL^{-1}) shows a pronounced frequency band for lower rigidities ($\leq$4.2 kPa), and dispersed frequency distribution for higher rigidities ($\geq$4.3 kPa). The most stable frequency (cycle length) is seen for tissue cultured on substrates with rigidity of 4.2 kPa. (F) Maximum of the combined power spectrum (most stable CL occurrence) dependent on the substrate rigidity. A local maximum can be found at approx. 4.2 kPa, which is consistent with the cell rigidity of 4.4 $\pm$ 0.6 kPa determined by AFM indentation measurements on glass substrates.

Figure 3.

The normalized histogram of CTD and CTI of each wave shows stabilization when the substrate rigidity goes below the cell rigidity. (A) Shows relative CTD-CTI occurrence for soft substrates with rigidities smaller than

4.25 kPa. (B) Shows relative CTD-CTI occurrence for hard substrates with rigidities larger than 4.25 kPa. (C) Shows relative CTD-CTI occurrence for all substrates. (D) Shows the histogram of cycle length (CL=CTD+CTI) distribution for soft and hard substrates in red and green color with an average CL of (437 ± 35) ms and (437 ± 55) ms, respectively.

Figure 4.

Calcium transient alternans of high-frequency-paced cardiac tissue shows a peak at substrate rigidity of 4 kPa. (A to C) Typical data obtained from cultured cell tissue at a substrate rigidity of 3.5 kPa. (A) Restitution curve showing calcium transient alternans induced at a pacing period of approximately 400ms. (B) CTD versus CTI plot of waves (red circles) observed with an estimated critical pacing period T_c (blue square). (C) T_c is estimated by considering the variance of CTI. (D) Mean T_c vs. substrate rigidity. A local maximum is observed at approximately 4 kPa, which is consistent with the cell rigidity of 4.4 ± 0.6 kPa determined by AFM indentation measurements on glass substrates.

Figure 5.

Influence of rigidity matching in an one dimensional array of computed cells. (A) Shows the idealized system with $I_n = I_c = 0$. (B) Shows the system with no coupling $I_c = 0$ and Gaussian noise $I_n \neq 0$. The influence of noise leads to failure of wave propagation in the excitable part of lattices. (C) Shows the system with coupling $I_c \neq 0$ and Gaussian noise $I_n \neq 0$. The influence of coupling leads to stabilization of the conduction system and less propagation failure are observed. (D) Maximum of power spectrum depending on substrate rigidity in numerical simulations that assumes coupling $I_c \neq 0$ and Gaussian noise $I_n \neq 0$.

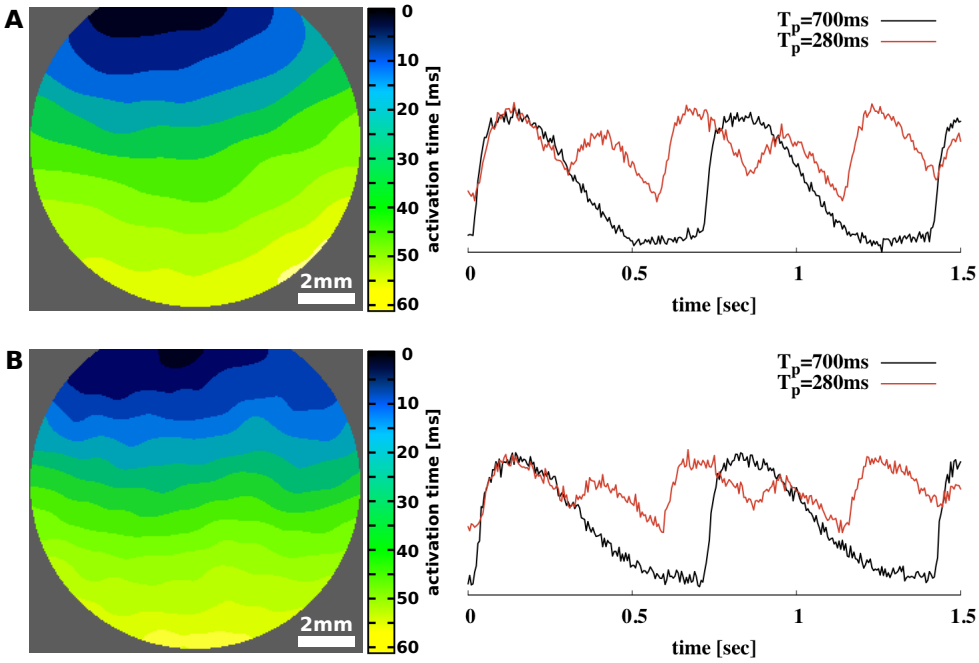

Figure 1:

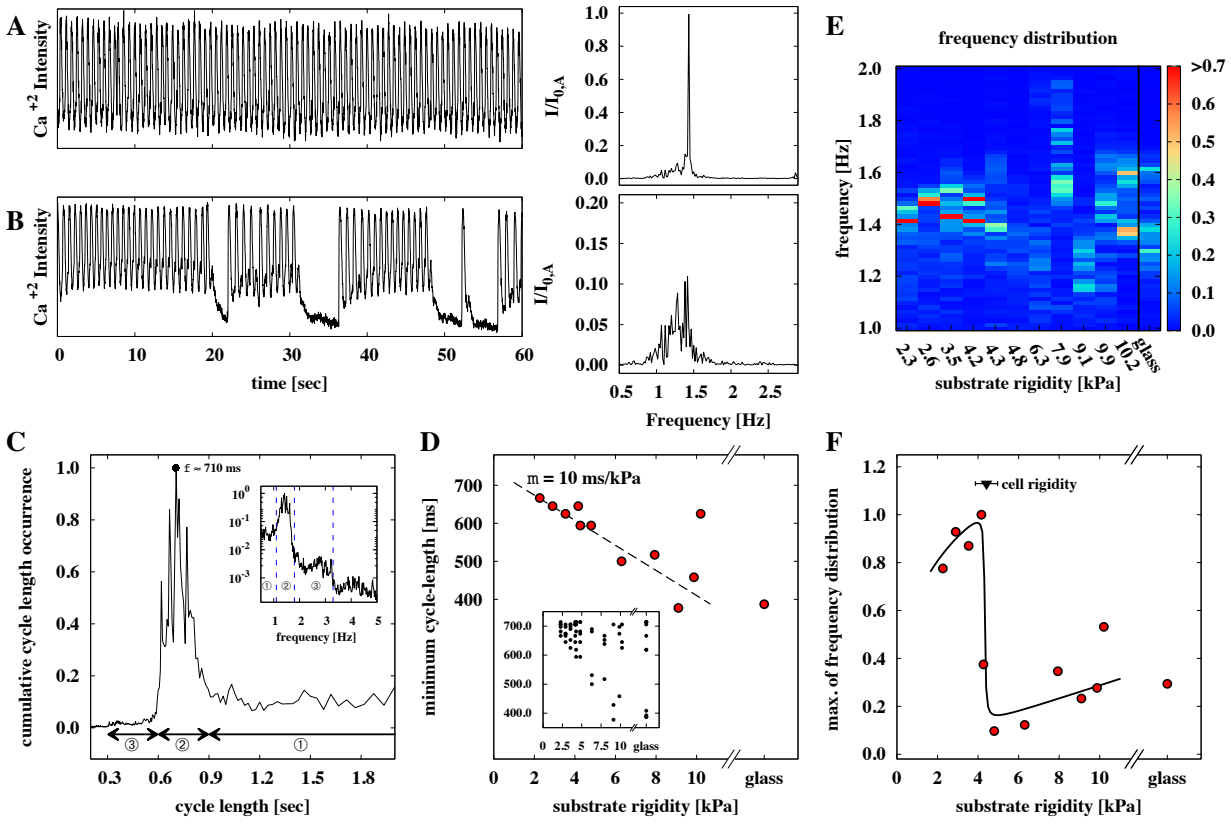

Figure 2:

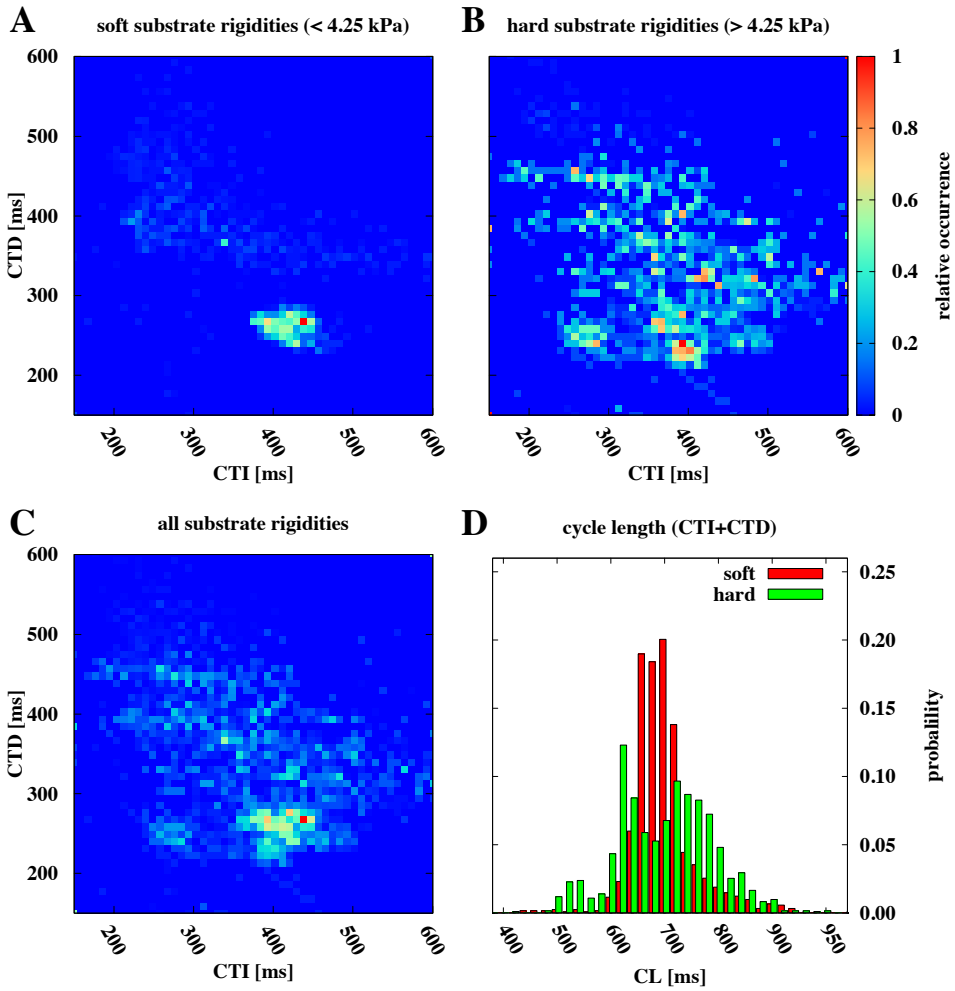

Figure 3:

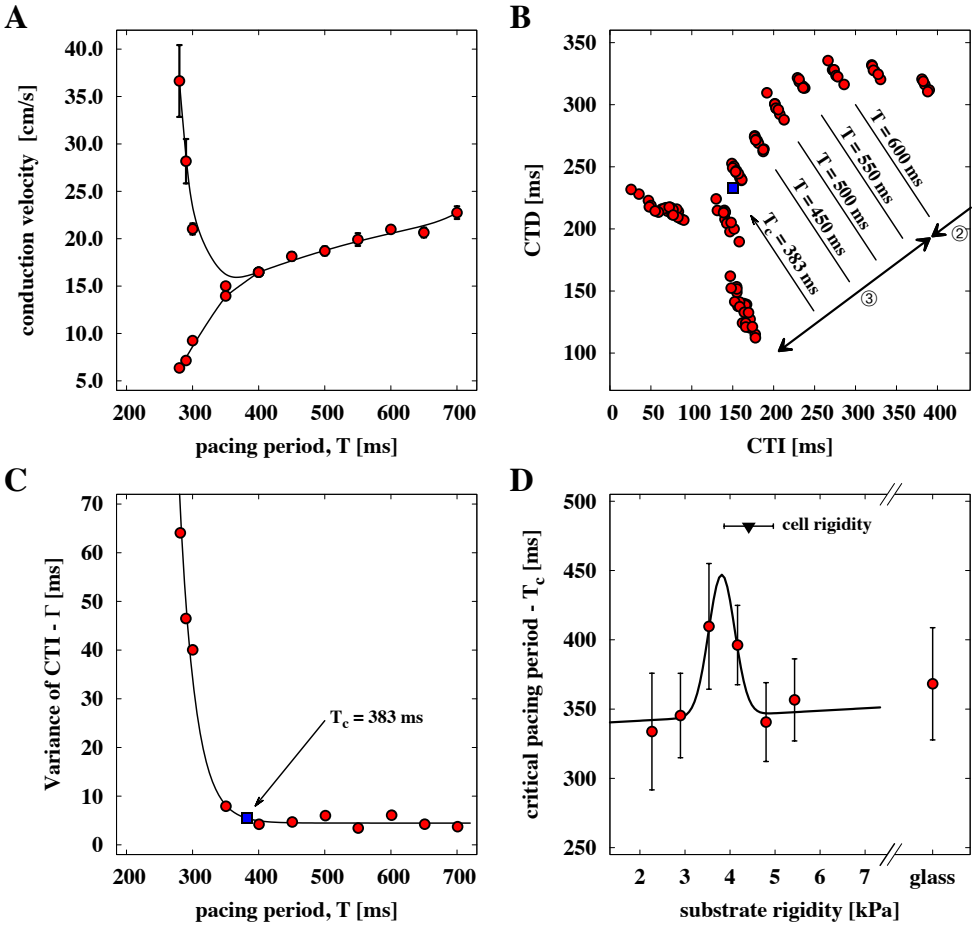

Figure 4:

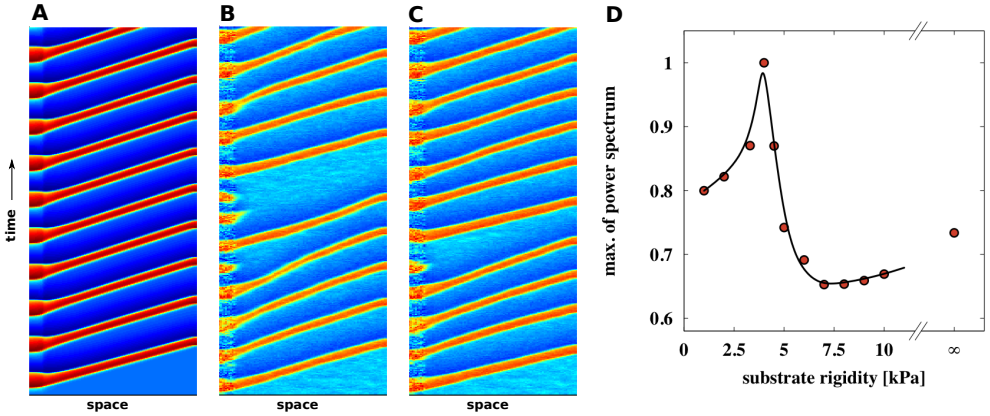

Figure 5: